RESERVE THIS SPACE

Spatial Heterogeneity in Ionic Liquids

Yanting Wang, Wei Jiang, and Gregory A. Voth

Center for Biophysical Modeling and Simulation and Department of Chemistry, University of Utah, 315 South 1400 East Room 2020, Salt Lake City, Utah 84112-0850

Electronically polarizable atomistic molecular dynamics models have been developed for the 1-alkyl-3-methylimidazolium nitrate ionic liquids with the alkyl-chain length ranging from 2 to 12. The molecular dynamics simulations with these models confirm the spatial heterogeneity previously discovered by the multiscale coarse-grained models (Wang & Voth, *J. Am. Chem. Soc.* 2005, *127*, 12192). The global structures are monitored by a heterogeneity order parameter. The tail groups of cations are found to aggregate and distribute more heterogeneously than the headgroups of cations and the anions, forming discrete tail domains. The anions always stay close to the headgroups. The charged groups retain their local structures relatively unchanged, forming a continuous polar network, and leading to different global structures when varying the side-chain length. The ionic diffusion is slower with increasing alkyl-chain length. Based on these simulation results, a refined mechanism can be proposed, considering the competition among the Coulombic interactions, the collective short-range interactions, and the geometrical constraint from the intramolecular bonds. This mechanism can explain many experimental and simulation results, and is expected to be general for most kinds of ionic liquids. The finite size effects due to the limited simulation size are also discussed.

Introduction

Understanding the structural properties of ionic liquids is essential for the systematic design and application of ionic liquids.

RESERVE THIS SPACE

Ionic liquids are room temperature molten salts which may be used as a potential substitute for the traditional environment-unfriendly organic solvents. They have a much lower melting point compared to the inorganic molten salts, which is achieved by involving a bulky organic cation (*1*). Generally most of the partial charges on the cation are distributed around its headgroup. When the side chain is short, the tail groups also have non-zero effective partial charges. With increasing side-chain length, the partial charges on the tail groups become smaller, and the amphiphilic feature for cations increases accordingly. Because there are numerous ionic liquid systems (*2*) to be chosen from to meet specific applications, a theoretical understanding of the "tunability" of ionic liquids, such as the changes of their physical properties with various side-chain lengths, is important for guiding their efficient design and applications.

Experiments have been done to investigate the behavior of ionic liquids with various cationic side-chain lengths. A liquid crystal phase has been observed for pure ionic liquids with long side chains (*3-6*). This mesophase affects the selectivity of the reaction products taken in ionic liquids *(6)*. Tokuda *et al*. (*7*) reported for $[C_nMIM]^+(CF_3SO_2)_2N^-$ that the summations of the diffusion coefficients for the cations and the anions follow the order $C_2 > C_1 > C_4 > C_6 > C_8$. (Here and thereafter, C_n refers to the ionic liquid system having an imidazolium cation with *n* carbon groups on its side chain.) Seddon *et al*. (*8*) and Huddleston *et al*. (*9*) reported similar experimental results for the systems with different anions. The above three papers (*7-9*) have also found a decreasing mass density with increasing side-chain length. Wakai *et al*. (*10*) observed that the dielectric constant of ionic liquids decreases with increasing side-chain length of cations. Bonhôte *et al.* (*11*) also studied the importance of viscosity and ion size on conductivity of ionic liquids.

Molecular dynamics (MD) simulations have also been done to computationally investigate this issue. By MD simulations, Urahata and Ribeiro found that the diffusion increases from C_1 to C_4, and then decreases when the side chain is longer (*12*). With static structure factor calculations, the same authors found a long-range ordering in their MD results (*13*). The MD simulations by Margulis (*14*) found that the systems are more structured with longer side chains. Del Pópolo and Voth (*15*) found evidence for dynamical heterogeneity, which should be indirectly related to spatial heterogeneity. Most recently Lopes and Pádua (*16*) used an all-atom model to report the microscopic separation of polar and nonpolar domains in ionic liquids. However, the authors did not give a clear mechanism to systematically explain their simulation results.

Recently we have successfully applied the multiscale coarse-graining (MS-CG) approach (*17, 18*) to the $EMIM^+NO_3^-$ (C_2) ionic liquid (*19*). The MS-CG model for $EMIM^+NO_3^-$ was then extended to qualitatively study the physical properties of ionic liquids with various lengths of side chains. By using these MS-CG models, we have revealed the spatial heterogeneity in ionic liquids formed by the aggregation of tail groups on side chains (*20*). The suggested mechanism is that the competition between the electrostatic interactions among the charged groups and the collective short-range interactions among the neutral tail groups results in the aggregation of tail groups, while the headgroups distribute as uniformly *as possible* (which does not mean completely uniformly). To verify the above mechanism, in this study polarizable atomistic models with full atomic detail have been developed for imidazolium cations with various side-chain lengths along with extensive MD simulations. In the past, we have shown (*21*). that electronic polarizability can be important to include in atomistic MD simulations.

In this work, our approach (*21*, *22*) for developing the polarizable model for C_2 has been applied to develop the all-atom models for C_4, C_6, C_8, C_{10}, and C_{12}. Here only cations with even number carbons on the alkyl chain have been studied, because those with odd number carbons are more expensive to prepare in experiments, and they have different trends for some physical properties (*5*). The MD simulations have then been carefully carried out to ensure that the systems with 512 ion pairs have good equilibration at $T =$ 400 K. It has been found that, with increasing cationic side-chain length, the system mass density and the diffusion of both the cations and the anions decrease; the tail groups aggregate to form isolated tail domains; and the charged groups retain their local structures relatively unchanged for different systems. By using a newly defined heterogeneity order parameter, the degrees of heterogeneous distribution have been quantified for different atom groups. With increasing side-chain length, both the headgroups and the tail groups distribute more heterogeneously. However, the tail groups distribute more heterogeneously than the headgroups of cations and the anions for all systems. Based on these observations, a mechanism is proposed to refine our previous one[20] based on the MD simulations using the MS-CG models.

Models and Methods

In this section the procedure of building the polarizable atomistic models is first described. A heterogeneity order parameter is then defined, deigned to quantify the spatial heterogeneity in a finite-size simulation box. What follows are the definitions for diffusion constant and radial distribution function. Finally the MD simulation procedure for equilibration and sampling is given.

Polarizable atomistic models

A polarizable atomistic model (*21*, *22*) has been developed for the $EMIM^+NO_3^-$ ionic liquid, based on the AMBER force field (*23*). In this model, a fast extended Lagrangian approach (*24*) similar in spirit to the Car-Parrinello method (*25*) has been used to treat the many-body polarizable model. In this method, the induced dipole degrees of freedom are coupled to a heat bath with a very low temperature (~ 0.1 K) separated from the system heat bath to help keep them evolving on the adiabatic surface. This algorithm leads to an increased simulation time (about a factor of two for C_2), but the polarization caused by the induced dipoles has been shown (*21*, *22*) to have a significant influence on both the structural and the dynamical properties of ionic liquids, and is thus considered to be essential. The polarizable model also brings the atomistic simulation results into closer agreement with the experimental data in the cases we have examined (*21*, *22*).

The total potential of the polarizable model V_{pol} is the sum of the bonded interaction, V_b, the short-range van der Waals interaction, V_{VDW}, the long-range Coulomb interaction , V_{el}, and an induction term, V_{ind}, i.e.,

$$V_{pol} = V_b + V_{VDW} + V_{el} + V_{ind} \qquad (1)$$

The bonded interaction V_b generally has the typical bond, valence angle, and dihedral angle terms among atoms

$$V_b = \sum_{bonds} \frac{1}{2} k_r \left(r - r_0\right)^2 + \sum_{angles} \frac{1}{2} k_\theta \left(\theta - \theta_0\right)^2 + \sum_{dihedrals} V_n \left[1 + \cos\left(n\phi - \gamma\right)\right] \qquad (2)$$

where k_r, k_θ, V_n are force constants, r, θ, φ are bond length, valence angle, and dihedral angle, respectively, r_0, θ_0, and γ are equilibrium positions, and n is an integer number.

The short-range interaction generally takes the 12-6 Lennard-Jones potential form

$$V_{VDW} = \sum_i \sum_{j>i} 4\varepsilon \left[\left(\frac{\sigma}{r_{ij}} \right)^{12} - \left(\frac{\sigma}{r_{ij}} \right)^{6} \right] \quad (3)$$

where ε is the depth of the energy minimum, σ is the minimum energy distance, r_{ij} is the distance between atom i and atom j.

In the Coulomb potential V_{el}, the charge q_i on atom i is the partial charge including the permanent dipole effect. The partial charges can be obtained from an *ab initio* study of the ions as described below, satisfying the constraint $\sum_i q_i = 1$ for cation, and $\sum_i q_i = -1$ for anion. With those partial charges, the Coulomb potential is written as

$$V_{el} = \sum_i \sum_{j>i} \frac{q_i q_j}{r_{ij}} \quad (4)$$

The induced term V_{ind} is expressed as

$$V_{ind} = -\sum_i \boldsymbol{\mu}_i \cdot \mathbf{E}_i^{\,0} - \sum_i \sum_{j>i} \boldsymbol{\mu}_i \cdot \mathbf{T}_{ij} \cdot \boldsymbol{\mu}_j + \sum_i \frac{\boldsymbol{\mu}_i \cdot \boldsymbol{\mu}_i}{2\alpha_i^{\,2}} \quad (5)$$

In the above equation $\mathbf{E}_i^{\,0} = \sum_{j \neq i} q_j \mathbf{r}_{ij} / r_{ij}^{\,3}$ is the electric field on atom i, generated by the partial charges of all other atoms, excluding those within the same ion of atom i. The dipole field tensor $\mathbf{T}_{ij}$ is calculated from the electrostatic potential $\varphi^f\left(\left|\mathbf{r}_i - \mathbf{r}_j\right|\right)$ at point j due to the charge at point i: $\mathbf{T}_{ij} = \nabla_i \nabla_i \varphi^f\left(\left|\mathbf{r}_i - \mathbf{r}_j\right|\right)$. The induced dipole moment is $\boldsymbol{\mu}_i = \alpha_i \left[\mathbf{E}_i + \sum_{j=1, j\neq i}^{N} \mathbf{T}_{ij} \cdot \boldsymbol{\mu}_j \right]$, where α_i is the atomic polarizability of atom i, $\mathbf{E}_i$ is the electric field on atom i. The isotropic atomic polarizabilities $\{\alpha_i\}$ are determined by fitting the anisotropic molecular polarizabilities of the ions, which can be obtained by an *ab initio* simulation. Note that the induced dipole on each atom depends on the positions of all atoms, so the polarizability is a many-body effect.

The polarizable atomistic models for C_4, C_6, C_8, C_{10}, and C_{12} were constructed by extending the force field parameters for C_2. The methylene groups were added to the cationic side chains. The standard AMBER force field parameters (*23*) for the bonded (bond, angle, and dihedral) interactions and the VDW interactions were assigned to the new degrees of freedom accordingly.

The isotropic atomistic polarizabilities fitted for C_2 (*19*, *22*) were assigned to the added atoms on the cations. These parameters are given in the Appendix.

The standard one-configuration two-step procedure (*26*) of fitting partial charges for the AMBER force field was followed to obtain the partial charges for those cations. The Gaussian package (*27*) was first used to obtain the *ab inito* optimized structure of the cations at the theoretical level of mp2/6-31g*. The same theoretical level was then used to obtain the partial charges fitted to the electrostatic potential at points selected according to the Merz-Singh-Kollman scheme (*28*, *29*). The RESP package as a part of the AMBER software was finally used to obtain the partial charges compatible to the AMBER force field parameters. Our fitted partial charges for C_4 are very close to those reported by de Andrade *et al.* (*30*). The fitted partial charges for the cations are also listed in the Appendix.

Heterogeneity Order Parameter

A new order parameter has been recently defined (*31*) to quantify the spatial heterogeneity continuously. This Gaussian-like *heterogeneity order parameter* (HOP) is defined for each site as

$$h_i = \sum_j \exp(-r_{ij}^2 / 2\sigma^2) \qquad (6)$$

where r_{ij} is the distance between sites *i* and *j*, corrected with the periodic boundary conditions, $\sigma = L / N^{\frac{1}{3}}$ with *L* the side length of the cubic simulation box and *N* the total number of the sites.

For a given configuration, the average HOP is computed by averaging over all N_s sites of interest, such that

$$\hat{h} = \frac{1}{N_s} \sum_{i=1}^{N_s} h_i \qquad (7)$$

The HOP is so defined that it is topologically invariant with the absolute distances between sites, thus independent of the simulation box size *L*. Because the weights of the sites far from the target site decrease quickly with distance, the HOP approaches a constant with increasing number of sites. Some ideal systems with $N = n^3$, n = 1, 2, 3, …, sites uniformly distributed in a cubic box were constructed, and the HOP was computed for these systems with periodic

boundary conditions applied. The values for the ideal systems $\hat{h}_0$ are given in Table I. The HOP takes a fixed number of 15.7496 when the number of sites is larger than 1000.

In order to let the HOP take some values around zero when the sites distribute almost uniformly, a *reduced* HOP for each configuration is defined as

$$h = \hat{h} - \hat{h}_0 \tag{8}$$

The HOP defined above actually characterizes the instantaneous density of sites. To measure the ensemble-averaged density of sites, a *lattice HOP* is defined to calculate the average density for all configurations from one constant *NVT* trajectory. In order to calculate the lattice HOP, the cubic simulation box is divided into small cubic cells. For one configuration, in each cell *i*, the lattice HOP c_i is the HOP averaged over all sites of interest in this cell, such that

$$c_i = \frac{1}{M}\sum_{j=1}^{M} \hat{h}_{ij} \tag{9}$$

Table I. Heterogeneity Order Parameter $\hat{h}_0$ for Uniformly Distributed Systems with Different Number of Sites N_s.

N_s	$\hat{h}_0$
1	1.0000
8	4.1464
27	10.8388
64	12.9513
125	15.3220
216	15.5285
343	15.7368
512	15.7431
729	15.7495
1000	15.7495
1728 and larger	15.7496

with *M* the number of sites in cell *i*, $\hat{h}_{ij}$ the HOP of the *j*th site in cell *i*. Note that the regular HOP $\hat{h}_{ij}$, rather than the reduced HOP h_{ij}, is used here, so that

the two cases of having no sites and having uniformly-distributed sites in a given cell are distinguishable.

If a cell contains no sites of interest, the lattice HOP in this cell takes the average value of all neighboring cells, weighted by the inverse value of their center-center distance, such that

$$c_i = \frac{\sum_{j=1}^{M_c} \frac{1}{r_{ij}} c_{ij}}{\sum_{j=1}^{M_c} \frac{1}{r_{ij}}} \qquad (10)$$

Here, M_c is the number of neighboring cells for cell i, c_{ij} is the lattice HOP for the jth neighbor of cell i, r_{ij} is the center-center distance from cell i to cell j. The neighboring cell is defined as the cells with their center-to-center distance from the target cell less than a cutoff of 5.9 Å, the same as that chosen in Ref. (*31*).

The ensemble-averaged lattice HOP $\langle c_i \rangle$ for cell i is the average value of instantaneous lattice HOP over all configurations for one trajectory, such that

$$\langle c_i \rangle = \frac{1}{N_t} \sum_{j=1}^{N_t} c_{ij} \qquad (11)$$

where N_t is the number of configurations, c_{ij} is the lattice HOP for cell i in the jth configuration. The ensemble-averaged lattice HOP for one trajectory is then obtained by averaging over all cells, given by

$$\langle c \rangle = \frac{1}{N_c} \sum_{i=1}^{N_c} \langle c_i \rangle \qquad (12)$$

where N_c is the number of cells in the system.

Diffusion and local structure

The mean square displacement of particles is defined as $\left\langle \Delta r^2(t) \right\rangle = \left\langle \left| \mathbf{r}_i(t_0 + t) - \mathbf{r}_i(t_0) \right|^2 \right\rangle$, with $\mathbf{r}_i$(t) the position of particle i at time t, averaged over all particles and initial times t_0. The diffusion constant is then calculated (*32*) by fitting the linear part of the mean square displacement $D = \frac{\left\langle \Delta r^2(t) \right\rangle}{6t}$. In this work, only the self-diffusivity of ions has been measured.

So the term "diffusion" will be unambiguously used to refer to the self-diffusivity of ions.

One widely-used method of characterizing the local structure of a liquid is through the radial distribution function (RDF), which is defined as (*32*),

$$g(r) = \frac{V}{N_s^2}\left\langle \sum_i \sum_{j \neq i} \delta\left(\mathbf{r} - \mathbf{r}_{ij}\right) \right\rangle \qquad (13)$$

where V is the system volume, N_s is the total number of sites, $\mathbf{r}$ is the radial distance, and $\mathbf{r}_{ij}$ is the distance vector between sites i and j. When the side chain is long, calculating the RDFs for the center of mass of the cations has less meaning. Alternatively the partial site-site RDFs between the center of masses of the subgroups of cations and the anions were calculated for ionic liquid systems.

Molecular Dynamics Procedure

With increasing cationic side-chain length, the number of atoms is larger with a given number of ion pairs, and the diffusion is slower (*7-9*). On the other hand, systems with longer alkyl chains may have a more significant finite size effect in a finite simulation box, which may be big enough for systems with shorter chains. Considering the above facts, obtaining the fully equilibrated ionic liquid systems with a reasonably large simulation size is not an easy task. In this study, a strategy aimed at accelerating the equilibration in the MD simulations is taken, as described below. The integration time interval of 0.45 fs for each MD step was used for all MD simulations.

An initial configuration containing 64 ion pairs was first manually constructed, with the ions periodically placed on the lattice positions in a very large cubic simulation box. The initial configuration was then equilibrated at T= 1000 K by a Hoover barostat (*33*) with a pressure of P = 1 atm for 10^6 steps (450 ps). At such a high temperature the memory from the initial configuration was easily lost. The equilibrated configuration at T = 1000 K was then cooled down sequentially to 400 K, with an interval of 200 K. At each temperature the system was equilibrated with the constant *NPT* simulation with P = 1 atm for 10^6 steps (450 ps). The obtained configuration at T = 400 K was then equilibrated at this temperature with the constant *NVT* simulation by a Nosé-Hoover thermostat (*34*), with the system density fixed to be the one averaged from the previous constant *NPT* simulation. This equilibration was done for more than 5×10^6 steps (2.25 ns). The final configuration was confirmed to be fully equilibrated by observing that the diffusion of ions reaches a constant value.

The fully equilibrated configuration with 64 ion pairs at T = 400 K was then duplicated once in each dimension to get an initial configuration with 512 ion pairs. This initial configuration then went through a constant *NPT* simulation with P = 1 atm at T= 400 K for 10^6 steps (450 ps) to allow the system to relax from the periodic image interactions in the smaller-size simulation, and to eliminate the margin area between the duplicated images. With the system size fixed to be that averaged from the above constant *NPT* simulation, the system with 512 ion pairs then underwent a production run with a constant *NVT* simulation at T = 400 K for 10^6 steps (450 ps). During this production run 1000 configurations were sampled evenly with a time interval of 0.45 ps.

Results

The procedure described in last section was performed to obtain the MD data for the ionic liquid systems C_2, C_4, C_6, C_8, C_{10}, and C_{12} with 512 ion pairs at T = 400 K. The finite size effect was first evaluated based on the C_6 systems with 64 and 512 ion pairs. Analyses were then performed for the obtained data to get the structural, dynamical, and thermodynamical properties. The heterogeneity order parameter was applied to these systems to quantify the global heterogeneity in the liquids.

Below the term “headgroup” is used to specifically refer to the imidazolium ring of the cation, and the term “tail group” is used to refer to the terminal methyl group of the alkyl chain on the cation. The term “polar group” refers to the anion in addition to the headgroup and the adjacent methyl and methylene groups with non-negligible net partial charges, while the term “nonpolar group” refers to the methylene and methyl groups on the alkyl chain with negligible net partial charges. Here a net partial charge on a group of atoms is considered to be negligible if its absolute value is smaller than 0.03 elementary charges, which, when apart about 5 Å from another group with the same type, roughly generates a Coulombic potential energy of less than 10% of the typical minimum short-range potential ~0.03 eV. The polar groups are dominated by the Coulombic interactions, while the nonpolar groups mainly have the collective short-range interactions. By this criterion, the third methylene group and other groups farther

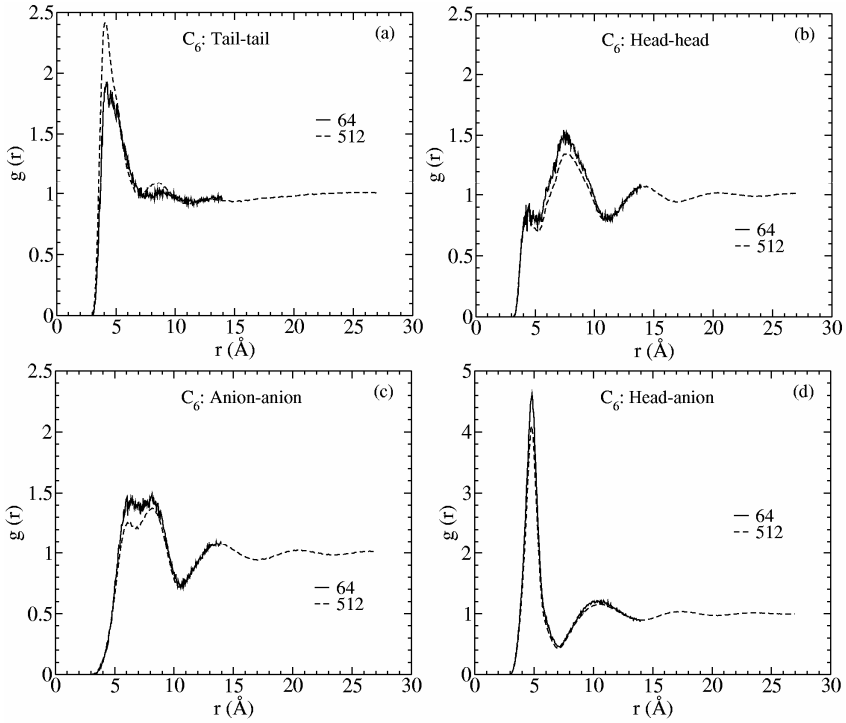

Figure 1. (a) Tail-tail, (b) head-head, (c) anion-anion, and (d) head-anion radial distribution functions for the C_6 systems with 64 and 512 ion pairs, respectively.

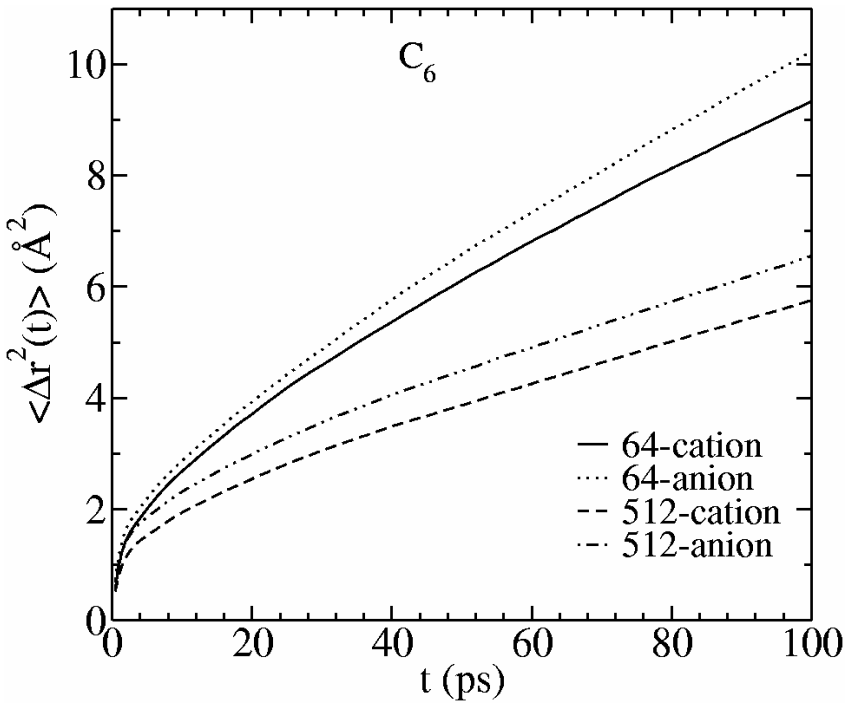

Figure 2. Mean square displacements for the C_6 systems with 64 and 512 ion pairs, respectively.

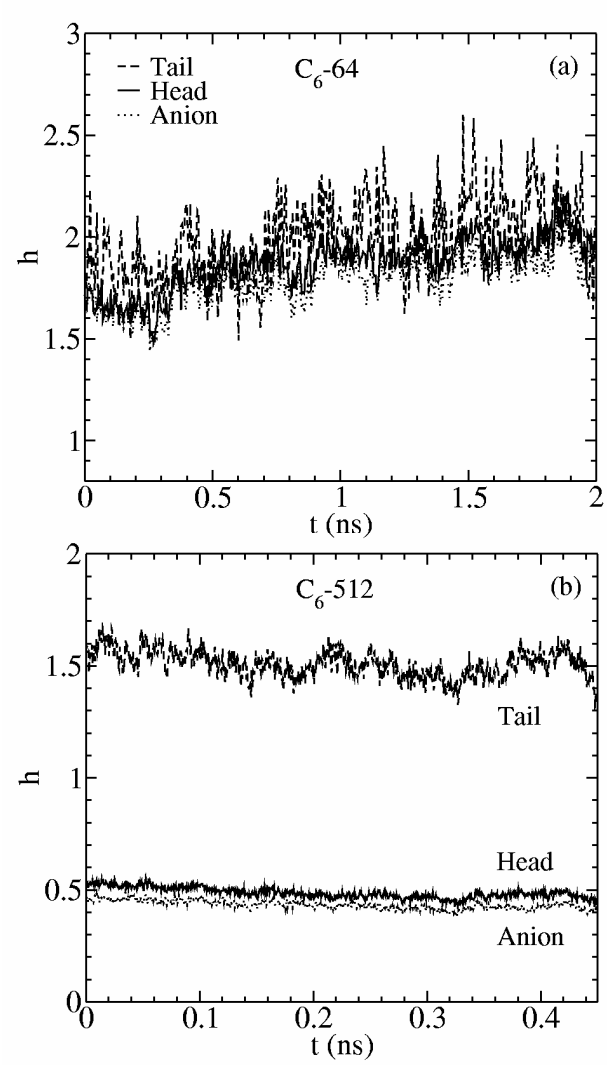

Figure 3. Instantaneous heterogeneity order parameter for the C_6 systems with (a) 64 and (b) 512 ion pairs, respectively.

from the imidazolium ring on the side chain are considered nonpolar, while the remaining groups of the cation are considered polar.

Finite Size Effects

For ionic liquids, the quantities of interest are the physical and chemical properties of macroscopic samples containing ~10^{23} molecules. In atomistic MD simulations with today's computers, however, only systems ~10^3 molecules with periodic boundary conditions can be studied. When the side length of the simulation box is smaller than twice the characteristic correlation length of interest, finite size effects will significantly distort the simulated properties. Generally the magnitudes of correlation lengths for different physical properties are not the same. Below the results for the C_6 systems with 64 and 512 ion pairs will be compared to show qualitatively different correlation lengths in ionic liquid systems.

In Figure 1 the RDFs between headgroups, tail groups, and anions for the C_6 systems with 64 and 512 ion pairs are compared. According to the four plots in Figure 1, while the peak positions remain the same, the finite size tends to suppress the peaks in the tail-tail RDF, but to raise the peaks in the head-head, anion-anion, and head-anion RDFs. This means that in an insufficiently large simulation box, the tail groups appear to distribute more uniformly, while the headgroups and anions appear to be more structured.

The mean square displacements for these two systems are shown in Figure 2. For both systems, the cations diffuse slower than the anions. This may be qualitatively understood by taking into account the fact that, besides the Coulombic interactions between the ions, the cations are also bound by the collective short-range interactions between the nonpolar groups. In contrast to the case of C_2 (*22*), the ions diffuse faster in the 64 ion-pair system than in the 512 ion-pair system. This is possibly due to the fact that the tail aggregation for C_6 in the smaller size system is reduced, as can be seen in Figure 1a.

Although quantitatively different, the RDFs and the diffusion for these two sizes give the same qualitative results for local structures and dynamics. In contrast, the finite size effect is so large for the global heterogeneity distributions in ionic liquids that the results from the small-sized systems would give a false impression. The reduced HOP defined in eq (8) was applied to these two C_6 systems, and their values are plotted in Figure 3. For the 64 ion-pair system, the HOPs fluctuate considerably and do not show much difference for the distributions of the tail groups from those for the headgroups and anions. For the

512 ion-pair system, however, the HOPs are stable and the tail groups take a value larger than those for the headgroups and the anions, indicating that the tail groups distribute more inhomogeneously. Thus the finite size effect has a large influence on the global heterogeneity of ionic liquids. It also likely suggests that the characteristic correlation length for global heterogeneity is longer than that for local structure and that for diffusion. It can be expected that, with increasing length of cations, the characteristic correlation length for heterogeneity becomes larger, and the required simulation size exhibiting little finite size effect should increase correspondingly.

In order to evaluate approximately the influence of the finite size effect on the systems with various lengths of the alkyl chain, the distributions of their cationic lengths d were calculated for 512 ion-pair systems. Here the cationic length d is defined as the distance from the center of mass of the methyl group not on the alkyl chain to the center of mass of the tail group. The distributions are shown in Figure 4. With increasing number of methylene groups on the alkyl chain, the most probable value of the cationic length d_M increases, but the probability of having this value decreases, and the distribution broadens, reaching very small values of d. This indicates that longer alkyl chains are more flexible and can bend to form many different shapes, so that the distance between the two terminals can range more widely.

The side length L of the cubic simulation box in the constant NVT simulations for the systems with 512 ion pairs was then divided by the most probable cationic length d_M. The plot of this ratio is drawn as the inset in Figure 4. The ratio decreases with increasing side-chain length, showing that, by taking the same simulation size of 512 ion pairs for all of the simulated systems, the finite size effect is more significant for the systems with longer side chain lengths. However, because no quantitative measurements have been done for the correlation lengths, no theoretical criterion can be used to gauge which systems are almost free of the finite size effect. Thus for the results shown below, the finite size effect is always considered in our data analyses.

Structural, Dynamical, and Thermodynamical Properties

The average mass densities obtained with 512 ion pairs are shown in Figure 5. Those obtained with 64 ion pairs are within 0.8% deviation from the data shown. The densities obtained for C_4 and C_6 are very close to the experimentally reported 1.1120 g/cm^3 for C_4 and 1.0769 g/cm^3 for C_6 at T= 90 °C (*8*). Thus the finite size effect should have little influence on the mass

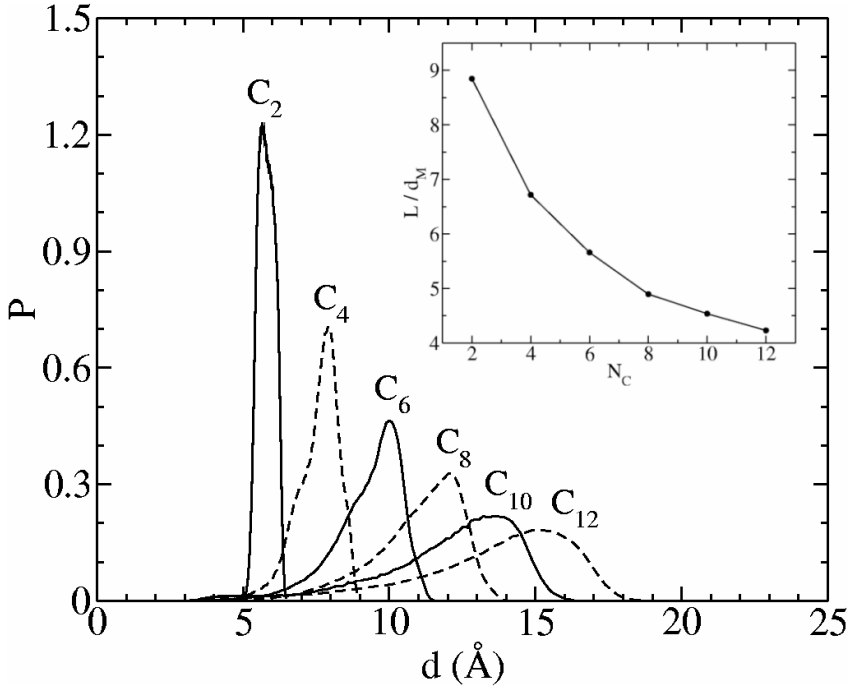

Figure 4. Distributions of cationic length for different ionic liquid systems. The inset is the ratio of the side length of the cubic simulation box with 512 ion pairs divided by the most probable cationic length, roughly showing the significance of the finite size effect.

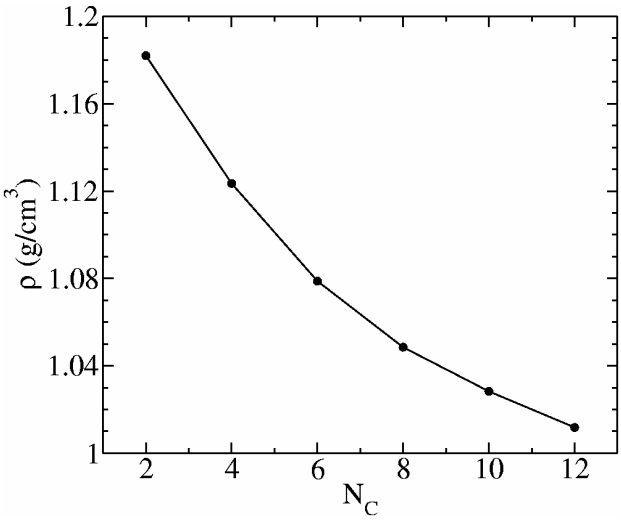

Figure 5. Mass densities for ionic liquids with various side-chain lengths.

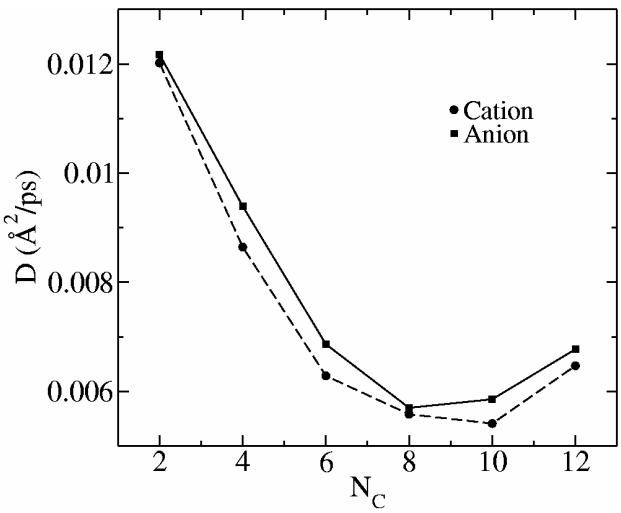

Figure 6. Diffusion constants for ionic liquids with various side-chain lengths.

density measurements. The density plot indicates that the mass density decreases as the alkyl chain length increases and approaches a constant value. This suggests that, at equilibrium, the methylene groups on the side chain have a larger space-to-mass ratio than the heavier head groups and anions. Increasing side-chain length includes more less-densely packed methylene groups in the cations. As the number of the methylene groups approaches infinity, the contribution from heavier atoms vanishes, and then the system density approaches a constant. The monotonic decrease of mass density with increasing alkyl chain length is consistent with the experimental observations (*7-9*).

The diffusion constants for different ionic liquid systems are shown in Figure 6. Since the product runs are relatively short, the obtained diffusion constants may not be very accurate. They are shown here to illustrate the qualitative trend of the diffusion with various side-chain lengths. For all systems, the cations move slower than the anions. With increasing side-chain length, the ions move slower, except C_{12} and the anion of C_{10}, which we believe is due to the finite size effect. The slow down of the diffusion can be qualitatively understood by noting that the collective short-range attractive interactions increase with longer side-chain lengths, and the attractive interactions bind the cations more tightly than the systems with shorter side chains. The tendency that longer chain systems diffuse slower has also been found in experiments (*7-9*).

In order to reveal the characteristics of the local structures, the site-site RDFs for different ionic liquid systems are shown in Figure 7. For all of the systems studied, the main peak for the tail-tail RDF is higher than that for the head-head and anion-anion RDFs, indicating that the tail groups aggregate more than the headgroups and the anions. From C_4 to C_8, with longer side chains, the main peak for the tail-tail RDFs is higher, showing that, for longer side-chain systems, more tail groups tend to aggregate. The characteristic second peak demonstrates an inhomogeneous distribution of the formed tail domains. Since the finite simulation size tends to lower the peak heights as shown in Figure 1a, the decrease of the peaks for C_{10} and C_{12} may be attributed to the finite size effect.

The head-head, anion-anion, and head-anion RDFs retain their shapes relatively unchanged for various systems. This means that the polar groups always retain their local structures, no matter how long the side chain is. We attribute this to the very strong Coulomb interactions between the headgroups and the anions. The peak heights for those RDFs grow with the length of the

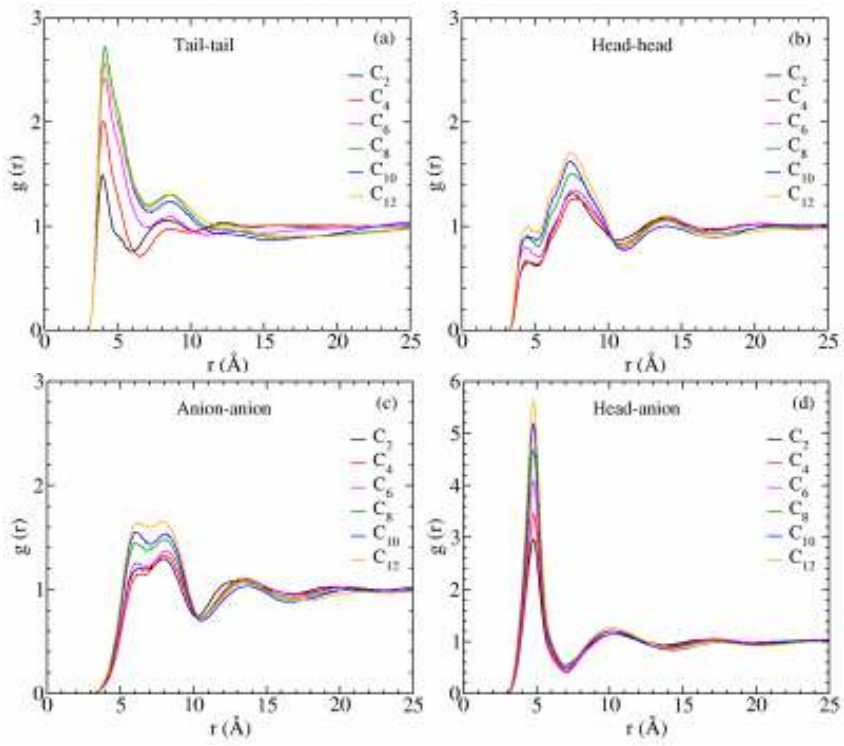

Figure 7. (a) Tail-tail, (b) head-head, (c) anion-anion, and (d) head-anion radial distribution functions for ionic liquids with various side-chain lengths.

alkyl chain. This may correspond to the slower diffusion for a longer side-chain system, so the system appears more structured. Nevertheless, the finite size effect might also contribute at this feature, since the finite system tends to increase the peak heights for those RDFs, as shown in Figure 1b—d. In Figure 7d the head-anion RDFs have a high peak at a short distance of about 5 Å. This is strong evidence that the anions are always distributed very closely to the headgroups, and the polar groups containing the headgroups and the anions are more localized in the longer side-chain systems.

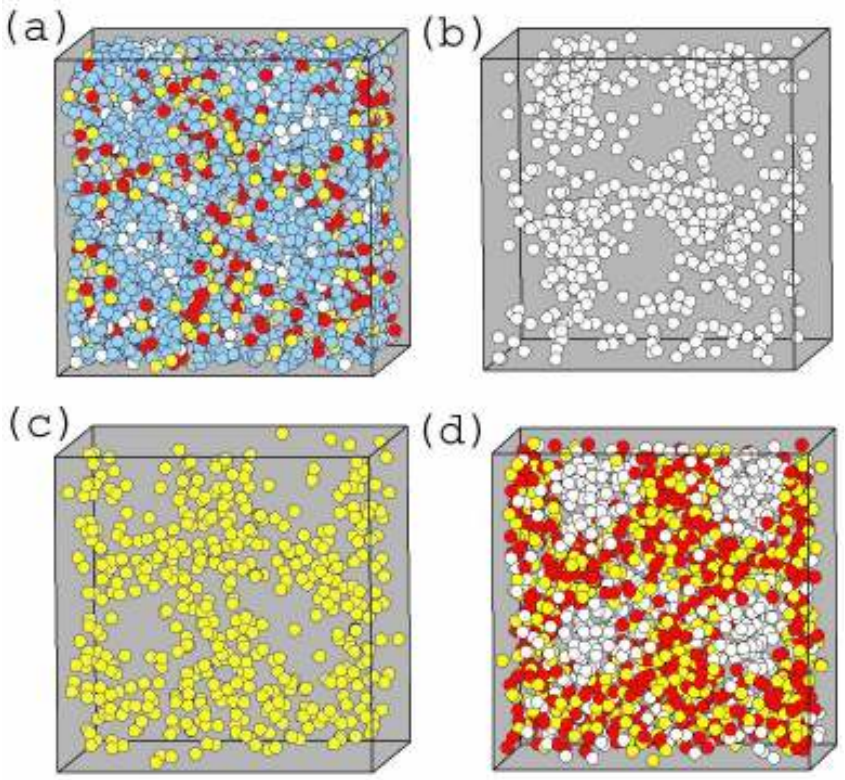

Figure 8. One instantaneous configuration showing the heterogeneous distribution of tail, head, and anion groups for the C_8 system with 512 ion pairs. (a) All atoms. (b) Tail groups only. (c) Headgroups only. (d) Tail groups (white), headgroups (yellow), and anions (red).

Spatial Heterogeneity

The above site-site RDFs reflect the local structures in the ionic liquids. The local distributions should in some ways relate to the global structures.

Below one representative configuration of C_8 is taken as an example to show the global heterogeneous distributions for different sites in a visual way. The heterogeneity order parameter is then calculated for all the systems to show the tendency of the global heterogeneous distributions with various cationic alkyl-chain lengths.

One instantaneous configuration of C_8 is shown in Figure 8. Consistent with the head-anion RDFs shown in Figure 7d, the anions always stay close to the headgroups. In order to retain their local structures, when the alkyl chain is long, the headgroups and the anions can not distribute as uniformly as they do in the C_2 system, but span to form an inhomogeneous network with vacancies, such that the nonpolar groups connected with the headgroups by the chemical bonds can fill in.

By visual examination of Figure 8b and c, the tail groups form tail domains, and distribute more heterogeneously than the headgroups, due to the collective short-range interactions. Although both the tail groups and the headgroups distribute heterogeneously, the mechanisms they follow are different. The tail groups "actively" take a heterogeneous distribution due to the collective short-range interactions between the nonpolar groups, while the polar groups "passively" distribute heterogeneously due to the Coulomb interactions retaining their local structures and the geometrical constraint coming from the long alkyl chains. The degree of heterogeneity for tail groups is always larger than that for polar groups. Looking back to Figure 4, it can be seen that the cations curl in some complicated ways to satisfy the equilibrium requirements for both the tail groups and the headgroups.

Figure 8d shows the same snapshot including the tail groups, the headgroups, and the anions. Because the headgroups and the anions are attracted by the strong electrostatic interactions to maintain their local structures, they form a continuous polar network, as observed previously by Lopes and Pádua (*16*). In contrast, the tail groups aggregate to form several discrete tail domains, surrounded by the continuous polar network.

The reduced HOP has been performed on all of the systems to get the instantaneous HOP values for tail groups, headgroups, and anions, similar to those shown in Figure 3b. The average values and their standard deviations for these instantaneous HOPs are plotted in Figure 9. For all of the systems, the average HOP for the tail groups is larger than that for the headgroups. This demonstrates that the tail groups always globally distribute more inhomogeneously than the headgroups. The average HOP for anion is very close to that for headgroups, because the anions are always very close to the headgroups. Except C_{10} and C_{12}, for which the finite size effect appears to be

significant, the average HOPs for both the tail groups and the headgroups increase. However, the reasons for this increase are different. With increasing

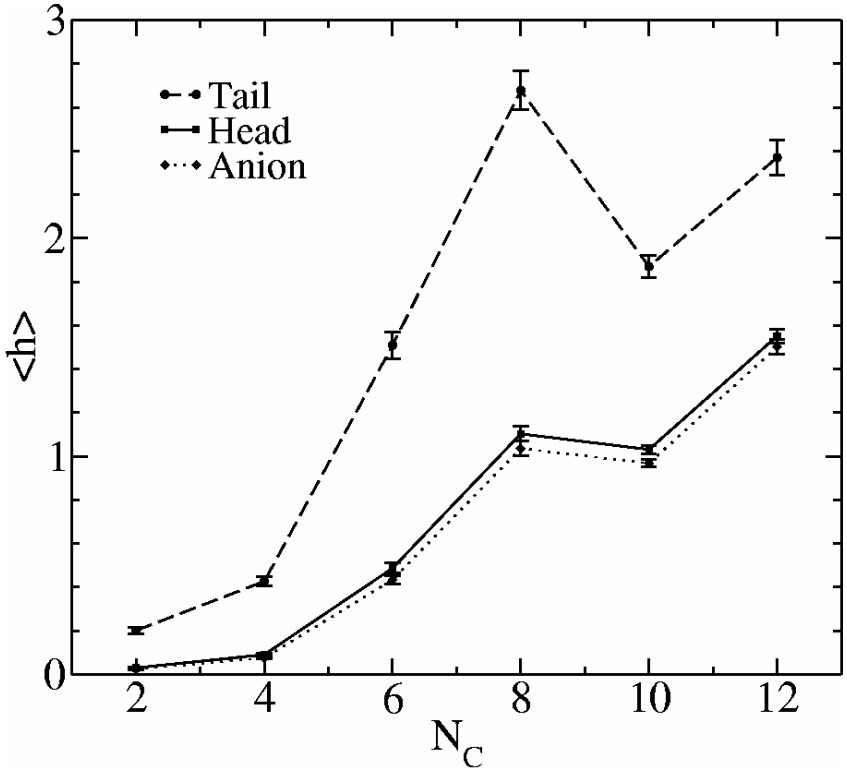

Figure 9. Average heterogeneity order parameters for the ionic liquid systems with various alkyl-chain lengths. The error bars are the standard deviations.

side-chain length, the tail groups distribute more heterogeneously because of the stronger collective short-range attractive interactions between the nonpolar groups. On the other hand, the more heterogeneous distribution of the headgroups is due to the fact that the growing size of the alkyl chains requires more space, so the requirement of maintaining the local structures forces the distribution of the polar groups to be more localized.

The behavior of the methylene groups on the side chain between the headgroups and the tail groups were then investigated. The methylene groups on the side chain of C_8 are denoted by M_n, where n is the position of the methylene group away from the headgroup. The RDFs between the same groups are drawn for M_2, M_4, and M_6 in Figure 10a. The RDFs for the headgroups and the tail groups are also plotted in the same figure for comparison. The main peak of the RDFs grows as the methylene groups come closer to the tail groups, showing that more groups aggregate. However, the RDFs are in no way similar to the RDFs for the tail groups of C_2, C_4, and C_6, as shown in Figure 7a.

The HOPs have also been calculated for M_2, M_4, and M_6 and are plotted in Figure 10b. The HOPs grow from M_2 to M_4 to M_6. They are all smaller than those for the tail groups, and only M_6 has larger HOPs than the headgroups. This suggests that the methylene groups in the middle of the side chains seem to act globally in a way compromising the heterogeneities in the two ends. It is interesting that the HOPs are very close to the values for the corresponding tail groups, i.e., M_2 takes the HOP values close to the tail groups of C_2, and vice versa, although their RDFs are quite different. This seems to suggest that, with a growing side chain, although the system volume expands, the existing groups on the side chain topologically retain their global heterogeneity. The additional nonpolar groups fill in the added space in a more aggregating manner. At the same time, the polar groups change their global distributions with their local structures unchanged. Below more analysis will be presented to make this point clear.

The HOP calculations shown above characterize the *instantaneous* spatial heterogeneity of individual atom groups. In order to see how the *ensemble-averaged* domains behave, the lattice HOP $\langle c_i \rangle$ was performed on the ionic liquid systems with different side-chain lengths. The three dimensional illustration of the lattice HOPs for the tail groups and the headgroups for C_2 and C_8 systems are shown in Figure 11. In these pictures, each small sphere represents the lattice HOP value in the corresponding cell. The warmer is the color, the larger the lattice HOP value. Figure 11a and b shows that, on average, both the tail groups and the headgroups in C_2 distribute almost uniformly, despite the fact that the tail groups have some instantaneous spatial heterogeneity, as seen in Figure 9. Nevertheless, Figure 11c and d have many highly populated cells as well as many poorly populated cells. This means that,

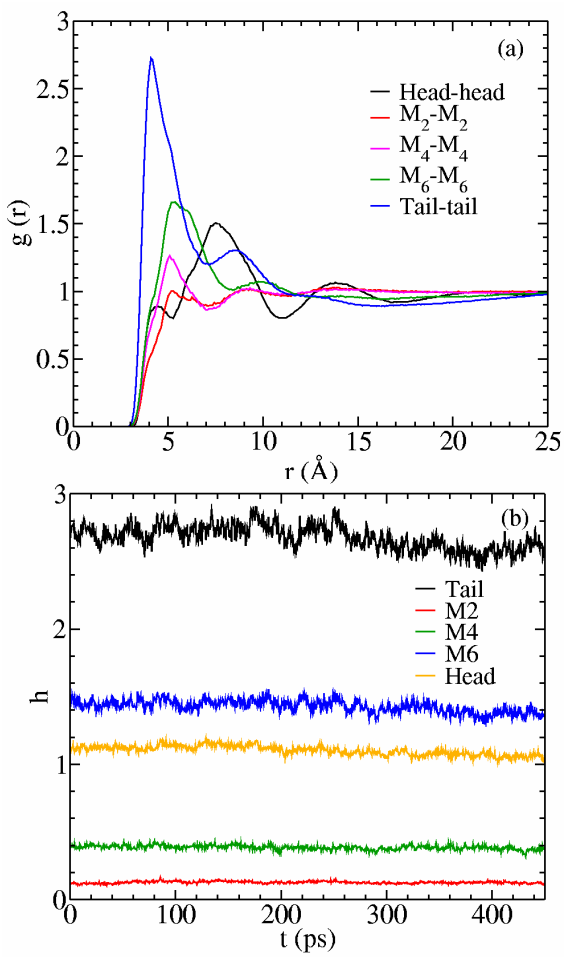

Figure 10. (a) Radial distribution functions and (b) instantaneous heterogeneity order parameter values for several atomic groups on the cations in the C_8 system.

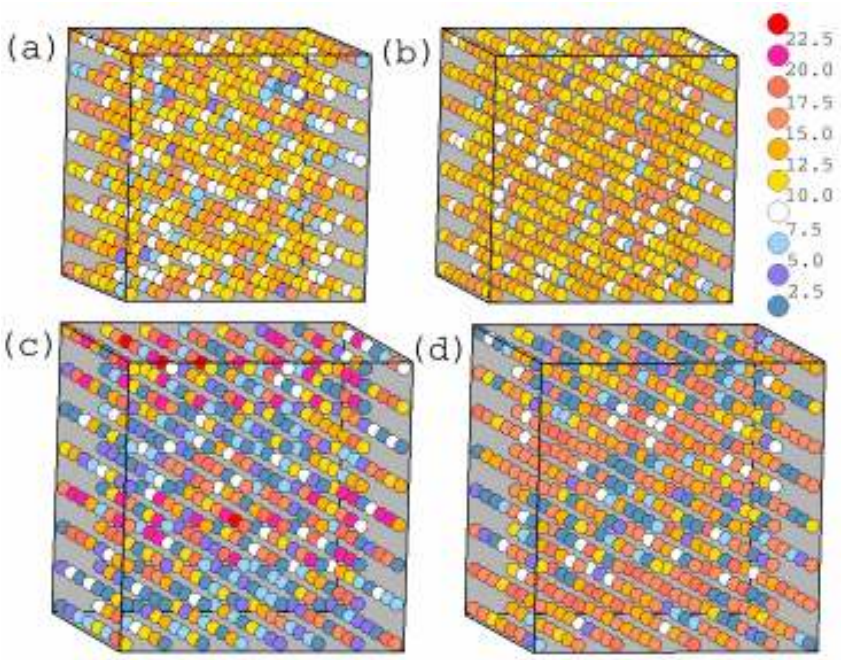

Figure 11. Three dimensional illustration of the lattice heterogeneity order parameters $\{\langle c_i \rangle\}$ *for (a) tail groups of* C_2*, (b) headgroups of* C_2*, (c) tail groups of* C_8*, and (d) headgroups of* C_8*. The spheres are colored according to the scale shown in this figure.*

even on average, the polar and tail domains in C_8 are distributed very non-uniformly.

By using the lattice HOP calculations, with the MS-CG models, we have qualitatively investigated (*31*) the phase transition of tail domains with increasing temperature. It has been found that, below the tail-domain-diffusion transition temperature, the tail domains formed have relatively unchanged positions; above the transition temperature, although the tail domains still form instantaneous domains, on average they distribute uniformly. In the all-atom simulations reported here, because the tail aggregation is stronger with longer side chain, it seems reasonable to assume that the longer-chain system has a higher domain-diffusion transition temperature. The pictures in Figure 11a and

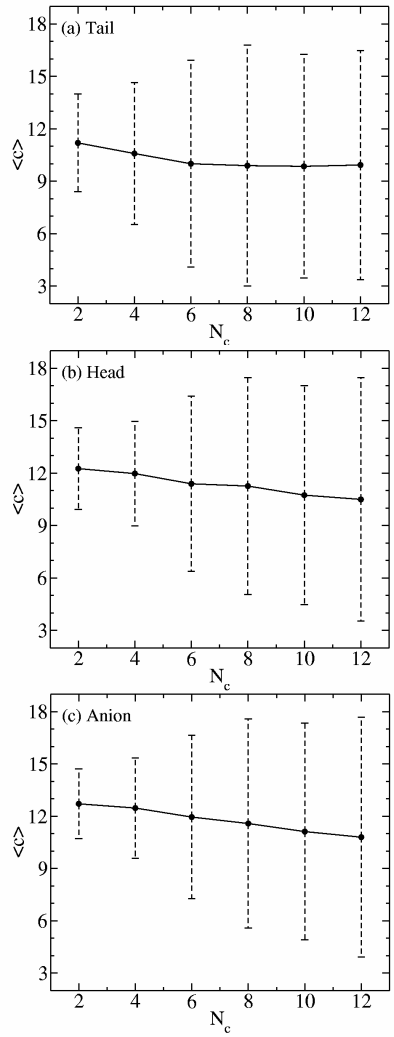

Figure 12. The average lattice HOP $\langle c \rangle$ *for (a) tail groups, (b) headgroups, (c) anions for different systems. The error bars are the standard deviations.*

c are very likely to suggest that the C_2 system at T = 400 K is above its tail-domain-diffusion transition temperature, while the C_8 system at T = 400 K is below its transition temperature. Although Figure 11b and d seem to suggest the same phenomena for headgroups, more work will be required to understand the phase behavior of the polar groups in ionic liquids.

The average lattice HOP averaging over all cells was calculated to show the trend of ensemble-averaged spatial heterogeneity with increasing side-chain length. The average lattice HOPs for tail groups, headgroups, and anions are shown in Figure 12. The error bar on each point indicates its standard deviation. From C_2 to C_8, the standard deviations grow for all three groups, meaning that the lattice HOP values are more different for longer side-chain systems. This indicates that, with increasing side-chain length, both the tail groups and the polar groups form more stationary domains. For the C_{10} and C_{12} systems, the finite size effect surely suppresses their standard deviations.

Mechanism

The results obtained by the all-atom polarizable models qualitatively agree with those by the primitive MS-CG models, but coincide more quantitatively with experimental results. A refined mechanism is thus proposed here to explain the behavior of ionic liquids with various lengths of cationic side chain. The main difference of this mechanism from our previous one (*20*) is the behavior of the polar groups. In this study the headgroups are found to retain their local structures, due to the very strong Coulombic interactions with the anions, rather than to push each other away as far as possible. Similar behavior has been suggested by the simulations of Lopes and Pádua (*16*).

There are mainly two kinds of competing non-bonded interactions between ions in ionic liquids: The Coulombic interactions and the collective short-range interactions. For the polar groups, the Coulomb interactions are very strong, such that the short-range interactions are only significant when the groups come very close and the short-range interactions are repulsive. The Coulomb interactions dominate the local behavior of the polar groups. These interactions are so strong that the polar groups retain their local structures and form continuous polar domains in different ionic liquid systems with various side-chain lengths (*16*). By contrast, the Coulomb interactions on the nonpolar groups are negligible compared to their collective short-range interactions. The tail groups distribute with their average distance around the equilibrium distance of the collective short-range interactions. Because the headgroups and the tail groups are

connected by chemical bonds, the competition of these two groups leads to a balanced spatial distribution of ionic liquids, in which the tail groups of cations tend to aggregate to form isolated tail domains, while the polar groups adjust their global behavior to retain their local structures. The methylene groups between the headgroups and the tail groups adjust their structures in some complicated ways to compromise the different requirements from the two ends but, in general, the closer they are to the tail groups, the more heterogeneously they distribute. However, they do not necessarily distribute more heterogeneously than the headgroups. Also due to the very strong attractive Coulomb interactions between the headgroups and the anions, the anions always distribute closely around the polar headgroups.

With longer side-chain length, the collective short-range interactions from the nonpolar groups are larger, leading to more aggregated domains of the tail groups. On the other hand, more methylene groups on the side chains require larger portions of the space to be filled in by them. Along with the requirement that the local strucutures of the polar groups remain unchanged, the distribution of the headgroups is more localized, resulting in a more localized continuous polar network. Nevertheless, the distribution of the tail groups is more heterogeneous than the headgroups, no matter how long the side chain is.

It should be noted that the above mechanism should be somehow modified to describe the C_2 system, in which the tail groups still have a non-negligible partial charge distribution, such that the short-range interactions do not dominate. Nevertheless, by calculating the average HOPs as shown in Figure 9, the tail groups in C_2 have also been found to distribute more heterogeneously than the headgroups. This may result from a subtle balance between the repulsive and attractive Coulombic interactions between the whole cations and the anions, considering the tail groups have a much smaller partial charge than the headgroups. The short-range interactions between the tail groups, which are comparable to the Coulombic interactions, might have some influence as well.

Our all-atom simulations with the polarizable models also give more evidences to support the tail aggregation (*20*) and domain diffusion mechanism (*31*) based on the primitive MS-CG models. They also suggest that the domain-diffusion transition temperatures are higher for longer side-chain systems. Atomistic simulations at different temperatures will likely be necessary to quantitatively investigate in detail the phase behavior of the polar and nonpolar domains in ionic liquids.

With this tail aggregation mechanism, some experimental results can immediately be rationalized, despite the fact that many experiments were done for ionic liquids with anions other than nitrate. The competition between the

different distributions of tail groups and headgroups results in a liquid crystal-like structure similar to those observed in experiments (*3-6*). The experimentally observed heterogeneity, however, is at mesoscopic scales and with longer side chains ranging from C_{12} — C_{18}. More quantitative comparisons can only be obtained when simulations are performed at a much larger scale with longer side chains than the current study.

When the alkyl chain is short, the cations distribute almost uniformly in the space, so the diffusing behavior of the ions is similar to simple isotropic liquids. With a longer alkyl chain, the heterogeneously distributed domains formed by the tail groups bind groups of cations together instantaneously, effectively adding an energy barrier between cation groups. Thus the ions move in a more hop-like fashion (*15*) rather than the free style in a simple liquid. The longer the alkyl chain is, the higher the energy barrier, and the slower the diffusion. The contribution from the polar groups is almost fixed since their local structures remain relatively unchanged. This explains the experimentally observed diffusion decrease, or equivalently, viscosity increase, with longer alkyl chains (*7-9*). The diffusion of the anions is somehow associated with that of the cations, since they are attracted to be around the headgroups of the cations.

Wakai *et al.* (*10*) observed experimentally that the dielectric constant of ionic liquids decreases with increasing side-chain length of cations. This can be understood by noting that, with increasing side-chain length, the portion of nonpolar groups on the cations increases. Consequently the ionic liquid is more difficult to polarize.

One interesting experimental observation is that, for the ionic liquids with the different anion BF_4^-, the C_2 to C_9 systems have a very strong tendency to form glasses, and are very difficult to crystallize. In contrast, the C_{10} and longer side-chain systems are easier to crystallize. This phenomenon might be interpreted by our mechanism as follows: When the side-chain length is not very long, the Coulombic interactions dominating the polar groups and the collective short-range interactions dominating the nonpolar groups are comparable; the competition between these two different interactions leads to the self-generated glassy state independent of the cooling rate (*35*). When the side chain is long enough, the charged groups are greatly localized, so the global behavior of the system is dominated by the collective short-range interactions. The competition between these two interactions with different length scales is weaker, so the tendency of self-generation of the glassy state is attenuated.

Discussion and Conclusions

By using the newly developed all-atom polarizable models (*21*, *22*) based on the AMBER force field, the spatial heterogeneity in ionic liquids previously investigated (*20*) by the MS-CG models (*17-19*) has been confirmed. The tail groups are found to aggregate, while the polar groups retain their local structures relatively unchanged. A refined mechanism coming from the contribution from the Coulomb interaction, the collective short-range interaction, and the geometrical constraint from the chemical bonds has been proposed. The simulation results are quantitatively consistent with experimental ones, and the proposed mechanism can explain many experimental observations. Although our simulations have only been for the ionic liquid systems containing cations with an imidazolium ring and a nitrate anion, the mechanism should be applicable to most organic ionic liquids, independent of the specific choice of cation and anion species.

Our mechanism can also be reconciled with the MD simulation results of other researchers. Urahata and Ribeiro (*12*) found that the diffusion increases from C_1 to C_4, and then decreases when the side chain is longer. This is qualitatively consistent with the experiments and our simulations. The difference for C_2 and C_4 might be explained by the differences of the anions and the simulation model used. The MD simulations performed by Margulis (*14*) and Urahata and Ribeiro (*13*) found that the systems are more structured with longer side chains. These are also consistent with our simulations, and can be explained by the inhomogeneous distribution of tail groups and slower diffusion with increasing side-chain length due to the tail aggregation mechanism. Our spatial heterogeneity mechanism may also closely relate to the dynamical heterogeneity (*15*, *36*).

Lopes and Pádua (*16*) have reported some all-atom MD simulation results similar to ours for ionic liquids with different anions, which can also be interpreted by the refined mechanism proposed here. They imply that the continuous polar network is due to the hydrogen bonding. Although hydrogen bond network exists in both solid and liquid phases (*37-41*), our results suggest that it is the large ionic net charges, rather than the hydrogen bonds, that bind the polar groups together. The hydrogen bonds should instead have some influence on the details of the local structures of ions. Although these authors showed some evidences of tail aggregation, they did not investigate the isolated tail domains. The statistical characteristics of the tail and polar domains have been quantified in the present study by ensemble-average calculations using a recently defined heterogeneity order parameter. It should also be noted that finite size effect may also exist in their results, since they used smaller simulation sizes up

to 350 ion pairs. Since Lopes and Pádua used a non-polarizable atomistic MD model, it seems clear that the many-body polarization effect does not have a significant influence on the global spatial heterogeneity, although it does have an effect on the local structures and diffusion for ionic liquids.

With increasing alkyl-chain length, the diffusion at a given temperature is slower. On the other hand, ionic liquids with longer cationic side-chain lengths require larger simulation sizes to eliminate the finite size effect. In addition, the formation of tail domains may further complicate the phase diagram of ionic liquid systems. The complete phase diagram of ionic liquids along with the formation of a mesoscopic liquid crystal-like phase can only be studied with MD simulations in very large scales. Such simulations using all-atom models are far beyond the current computational capabilities. The MS-CG approach (*19*) for ionic liquids is therefore expected to be a powerful tool for the large scale simulations for ionic liquids. The phase diagram of ionic liquids may also be investigated by some analytical theories, similar to the methods used by Wolynes and co-workers (*35*, *42*) to study systems with competing interactions. This research is currently underway in our group.

Acknowledgments

This research was supported by the Air Force Office of Scientific Research (FA9550-04-1-0381). The authors thank Dr. Tianying Yan for useful discussions. Allocations of computer time from the National Center for Supercomputing Applications (NCSA), the Cray XT3 system at the Pittsburgh Supercomputing Center, and the Center for High Performance Computing at the University of Utah are gratefully acknowledged.

Appendix

A1. Isotropic Atomic Polarizabilities

The isotropic atomic polarizability α takes an identical value for the same type of atoms in one ion.

	Cation			Anion	
Atom	N	C	H	N	O
α	0.680	1.209	0.289	1.901	1.079

A2. Partial Charges of Atoms

A2.1. C2 and Nitrate

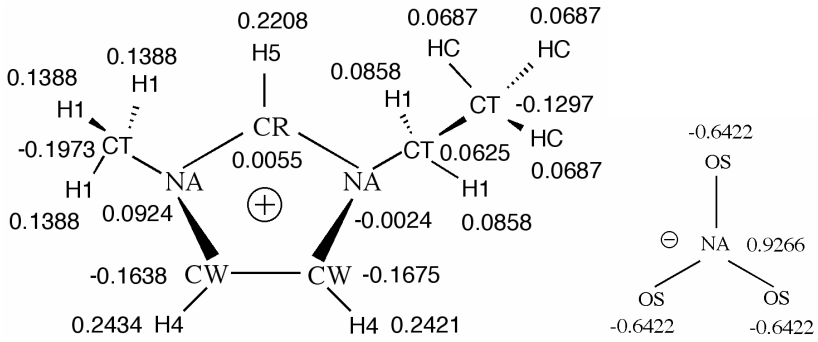

A2.2. C4

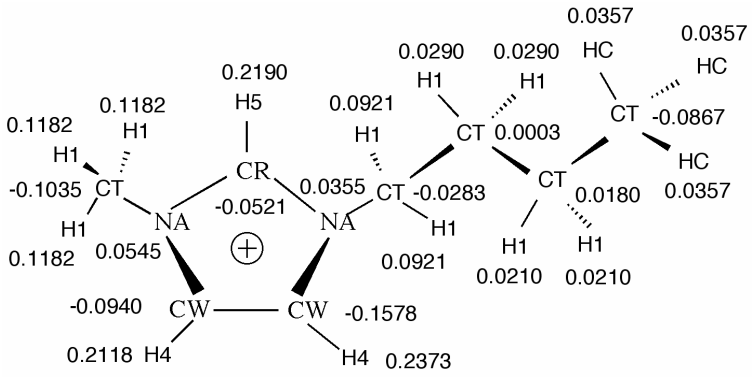

A2.3. C6

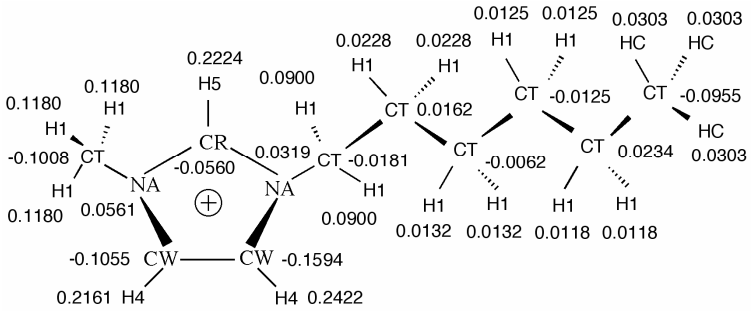

A2.4. C8

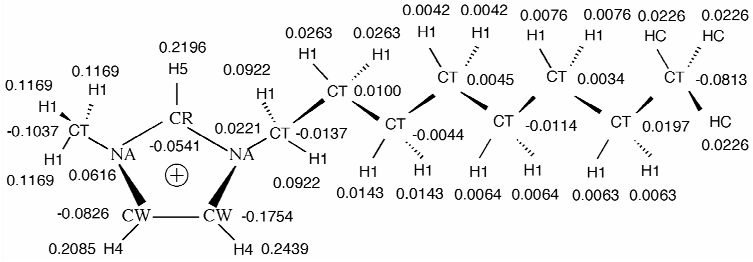

A2.5. C10

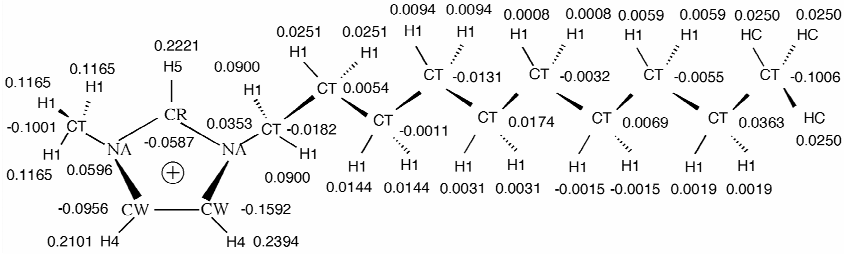

A2.6. C12

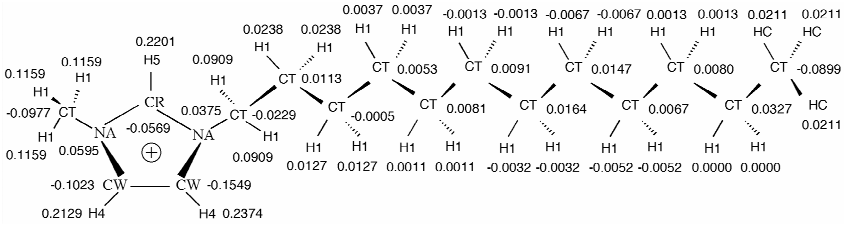

A3. Force Field Parameters

Bond parameters [k_r in kcal/(mol Å^2) and r_{eq} in Å].

bond	k_r	r_{eq}	bond	k_r	r_{eq}
CR-NA	954.0	1.343	CW-NA	854.0	1.381
CT-NA	674.0	1.475	CT-CT	620.0	1.526
CW-H4	734.0	1.080	CT-H1	680.0	1.090
CW-CW	1040.0	1.370	CR-H5	734.0	1.080
CT-HC	680.0	1.090	NA-OS	600.0	1.260

Angle parameters [k_θ in kcal/(mol radian^2) and θ_{eq} in degree].

angle	k_θ	θ_{eq}	angle	k_θ	θ_{eq}
CR-NA-CW	140.0	120.0	CW-NA-CT	140.0	125.8
NA-CR-NA	140.0	120.0	NA-CR-H5	70.0	120.0
NA-CW-H4	70.0	120.0	CW-CW-H4	70.0	128.2
NA-CT-H1	70.0	109.5	CT-CT-H1	100.0	109.5
H1-CT-H1	70.0	109.5	HC-CT-HC	70.0	109.5
CR-NA-CT	140.0	125.8	NA-CW-CW	140.0	120.0
NA-CT-CT	160.0	111.2	CT-CT-HC	100.0	109.5
CT-CT-CT	80.0	109.5	OS-NA-OS	300.0	120.0

Dihedral angle parameters [V_n in kcal/mol and γ in degree].

dihedral	V_n	γ	n	dihedral	V_n	γ	N
HC-CT-CT-NA	0.156	0.0	3	HC-CT-CT-H1	0.156	0.0	3
CT-NA-CR-H5	2.325	180.0	2	CT-NA-CR-NA	2.325	180.0	2
CT-NA-CW-CW	1.500	180.0	2	CT-NA-CW-H4	1.500	180.0	2
NA-CR-NA-CW	2.325	180.0	2	CR-NA-CW-H4	1.500	180.0	2
CW-NA-CR-H5	2.325	180.0	2	CR-NA-CW-CW	1.500	180.0	2
NA-CW-CW-NA	5.375	180.0	2	NA-CW-CW-H4	5.375	180.0	2
CT-CT-CT-H1	0.156	0.0	3	CT-CT-CT-CT	0.156	0.0	3
H1-CT-CT-H1	0.156	0.0	3	NA-CT-CT-CT	0.156	0.0	3
NA-CT-CT-H1	0.156	0.0	3	HC-CT-CT-CT	0.156	0.0	3
H1-CT-NA-CW	0.0	0.0	2	H1-CT-NA-CR	0.0	0.0	2
CW-NA-CT-CT	0.0	0.0	2	CR-NA-CT-CT	0.0	0.0	2
H4-CW-CW-	5.375	180.0	2	H5-CR-NA-	1.100	180.0	2

H4				NA[a]			
CR-CW-NA-CT[a]	1.100	180.0	2	H4-CW-CW-NA[a]	1.100	180.0	2
OS-OS-NA-OS[a]	50.000	180.0	2				

[a]Improper torsions.

Van der Waals parameters [ε in kcal/mol and σ in Å].

pair	ε	σ	pair	ε	σ
CW---CW[b]	0.0860	3.400	CW---NA	0.121	3.325
CW---H5	0.0359	2.911	CW---HC	0.0371	3.025
CT---CT	0.109	3.400	CT---H1	0.0418	2.936
CT---HC	0.0418	3.025	CT---H4	0.0404	2.955
CT---CW	0.0968	3.400	H1---H1	0.0160	2.471
H1---HC	0.0160	2.560	H1---H4	0.0155	2.491
H5---H5	0.0150	2.422	H5---HC	0.0155	2.536
H5---NA	0.0505	2.836	HC---HC	0.0160	2.650
HC---NA	0.0522	2.950	H4---H4	0.0150	2.511
CW---H1	0.0371	2.936	CW---H4	0.0359	2.955
CT---H5	0.0404	2.911	CT---NA	0.136	3.325
H1---H5	0.0155	2.446	H1---NA	0.0522	2.861
H5---H4	0.0150	2.466	HC---H4	0.0155	2.580
H4---NA	0.0505	2.880	OS---OS	0.170	3.001
NA---NA	0.170	3.250	NA---OS	0.170	3.125
H1---OS	0.0522	2.736	H4---OS	0.0505	2.756
CW---OS	0.121	3.200	CT---OS	0.136	3.200
H5---OS	0.0505	2.711	HC---OS	0.0522	2.825

[b]CR type atom has the same van der Waals parameters as CW atom.

References

1. Wasserschied, P.; Keim, W., *Angew. Chem., Int. Ed.* **2000,** 39, 3772.
2. Seddon, K. R., The International George Papatheodorou Symposium: Proceedings. In *Institute of Chemical Engineering and High Temperature Chemical Processes*, Boghosian, S., Ed. Patras, Greece, 1999.
3. Lee, K. M.; Lee, C. K.; Lin, I. J. B., *Chem. Commun.* **1997**, 899.
4. Gordon, C. M.; Holbrey, J. D.; Kennedy, A. R.; Seddon, K. R., *J. Mater. Chem.* **1998,** 8, 2627.
5. Holbrey, J. D.; Seddon, K. R., *J. Chem. Soc., Dalton Trans.* **1999**, 2133.
6. Lee, C. K.; Huang, H. W.; Lin, I. J. B., *Chem. Commun.* **2000**, 1911.
7. Tokuda, H.; Hayamizu, K.; Ishii, K.; Bin Hasan Susan, M. A.; Watanabe, M., *J. Phys. Chem. B* **2005,** 109, 6103.
8. Seddon, K. R.; Stark, A.; Torres, M.-J., Alternative Media for Chemical Reactions and Processing. In *Clean Solvents*, Abraham, M.; Moens, L., Eds. American Chemical Society: Washington D. C., 2002; Vol. ACS Symp. Ser. 819.
9. Huddleston, J. G.; Visser, A. E.; Reichert, W. M.; Willauer, H. D.; Broker, G. A.; Rogers, R. D., *Green Chemistry* **2001,** 3, 156.
10. Wakai, C.; Oleinikova, A.; Ott, M.; Weingärtner, H., *J. Phys. Chem. B* **2005,** 109, 17028.
11. Bonhôte, P.; Dias, A.-P.; Papageorgiou, N.; Kalyanasundaram, K.; Grätzel, M., *Inorg. Chem.* **1996,** 35, 1168.
12. Urahata, S. M.; Ribeiro, M. C. C., *J. Chem. Phys.* **2005,** 122, 024511.
13. Urahata, S. M.; Ribeiro, M. C. C., *J. Chem. Phys.* **2004,** 120, 1855.
14. Margulis, C. J., *Molec. Phys.* **2004,** 102, 829.
15. Del Pópolo, M. G.; Voth, G. A., *J. Phys. Chem. B* **2004,** 108, (5), 1744.
16. Lopes, J. N. A. C.; Pádua, A. A. H., *J. Phys. Chem. B* **2006,** 110, 3330.
17. Izvekov, S.; Voth, G. A., *J. Chem. Phys.* **2005,** 123, 134105.
18. Izvekov, S.; Voth, G. A., *J. Phys. Chem. B* **2005,** 109, 2469.
19. Wang, Y.; Izvekov, S.; Yan, T.; Voth, G. A., *J. Phys. Chem. B* **2006,** 110, 3564.
20. Wang, Y.; Voth, G. A., *J. Am. Chem. Soc.* **2005,** 127, 12192.
21. Yan, T.; Burnham, C. J.; Del Pópolo, M. G.; Voth, G. A., *J. Phys. Chem. B* **2004,** 108, (32), 11877.
22. Yan, T.; Burnham, C. J.; Wang, Y.; Gao, X.; Voth, G. A., *J. Phys. Chem. B (submitted)* **2006**.

23. Cornell, W. D.; Cieplak, P.; Bayly, C. I.; Gould, I. R.; Merz, K. M.; Ferguson, D. M.; Spellmeyer, D. C.; Fox, T.; Caldwell, J. W.; Kollman, P. A., *J. Am. Chem. Soc.* **1995,** 117, 5179.
24. Sprik, M., *J. Phys. Chem.* **1991,** 95, 2283.
25. Car, R.; Parrinello, M., *Phys. Rev. Lett.* **1985,** 55, 2471.
26. Case, D. A.; Pearlman, D. A.; Caldwell, J. W.; Cheatham, T. E., III; Ross, W. S.; Simmerling, C. L.; Darden, R. A.; Merz, K. M.; Stanton, R. V.; Cheng, A. L.; Vincent, J. J.; Crowley, M.; Tsui, V.; Radmer, R. J.; Duan, Y.; Pitera, J.; Massova, I.; Seibel, G. L.; Singh, U. C.; Weiner, P. K.; Kollman, P. A., *Amber 6*. University of California: San Francisoco, CA, 1999.
27. Frisch, M. J.; Trucks, G. W.; Schlegel, H. B.; et al., *Gausian 03*. Gaussian Inc.: Wallingford CT, 2004.
28. Besler, B. H.; Merz Jr., K. M.; Kollman, P. A., *J. Comp. Chem.* **1990,** 11, 431.
29. Singh, U. C.; Kollman, P. A., *J. Comp. Chem.* **1984,** 5, 129.
30. de Andrade, J.; Böes, E. S.; Stassen, H., *J. Phys. Chem. B* **2002,** 106, 13344.
31. Wang, Y.; Voth, G. A., *J. Phys. Chem. B* **2006,** In preparation.
32. Allen, M. P.; Tildesley, D. J., *Computer Simulation of Liquids*. Clarendon Press: Oxford, 1987.
33. Melchionna, S.; Ciccotti, G.; Holian, B. L., *Molec. Phys.* **1993,** 78, 533.
34. Hoover, W. G., *Phys. Rev. A* **1985,** 31, 1695.
35. Schmalian, J.; Wolynes, P. G., *Phys. Rev. Lett.* **2000,** 85, (4), 836.
36. Hu, Z.; Margulis, C. J., *Proc. Natl. Acad. Sci. USA* **2006,** 103, (4), 831.
37. Fannin, A. A.; Floreani, D. A.; King, L. A.; Landers, J. S.; Piersma, B. J.; Stech, D. J.; Vaughn, R. L.; Wilkes, J. S.; Williams, J. L., *J. Phys. Chem.* **1984,** 88, 2614.
38. Dieter, K. M.; Dymek, C. J.; Heimer, N. E.; Rovang, J. W.; Wilkes, J. S., *J. Am. Chem. Soc.* **1988,** 110, 2722.
39. Hardacre, C.; Holbrey, J. D.; McMath, S. E. J.; Bowron, D. T.; Soper, A. K., *J. Chem. Phys.* **2003,** 118, (1), 273.
40. Hayashi, S.; Ozawa, R.; Hamaguchi, H.-o., *Chem. Lett.* **2003,** 32, (6), 498.
41. Ozawa, R.; Hayashi, S.; Saha, S.; Kobayashi, A.; Hamaguchi, H.-o., *Chem. Lett.* **2003,** 32, (10), 948.
42. Wu, S.; Westfahl Jr., H.; Schmalian, J.; Wolynes, P. G., *Chem. Phys. Lett.* **2002,** 359, 1.